C. Zhao, M. Maestrini, P. Di Lizia
Low-Thrust Optimal Control of Spacecraft Hovering for Proximity Operations
Journal of Guidance Control and Dynamics, Vol. 47, N. 7, 2024, p. 1457-1469
doi:10.2514/1.g008063

Low-thrust optimal control of spacecraft hovering for proximity operations

Chuncheng Zhao *, Michele Maestrini†, and Pierluigi Di Lizia‡
Polytechnic University of Milan, Milan, Italy, 20156

I. Introduction

In recent decades, near-earth space missions such as on-orbit servicing and active space debris removal among others, have become increasingly desirable to expand the capabilities of human activities in space [1]. Spacecraft proximity operations, like rendezvous, inspection, and docking, play a vital role in these missions [2] and they are extensively studied among academic communities around the world. For such tasks, a waiting phase is paramount to gain time to receive commands or to gather information on the target satellite [3] while maintaining a safe distance. This phase, commonly called hovering [1], was preliminary conceived as a mission concept for station keeping about small bodies [4, 5]. Nonetheless, it has become a crucial preliminary task for proximity operations between satellites. During the hovering phase, the active spacecraft needs to control its trajectory to maintain the desired relative state and attitude so that it can perform a given function (e.g., inspection, pose estimation, etc. [6–8]).

From the current state of the art, two main strategies have been adopted to perform hovering. The first is to keep hovering at a fixed relative position around the target in the LVLH frame, whereas the second strategy tries to limit the relative trajectory in a bounded region. For the former, Dang et al. [9] studied the relative hovering control including J_2 perturbation. Further, Huang et al. [10] designed nonlinear control strategies for underactuated satellites using a sliding mode controller. Concerning the second approach, Irvin et al. [11] designed a periodic forced relative orbit (i.e., the teardrop orbit) inside a hovering zone using a purely geometrical approach and assuming the absence of orbital perturbations. To maintain this relative orbit a maneuver of a given amplitude is required after each orbital period. Consequently, the shape of the relative trajectory poses an upper limit on the duration of the mission given a certain mass budget. Alternatively, Deaconu et al. [12] found a natural relative orbit that satisfied both the boundary constraints of the desired hovering zone and a periodicity condition based on the parametric expressions of spacecraft relative trajectory [13]. In absence of perturbations this relative periodic orbit does not require controls, hence minimizing the fuel cost. Moreover, in [14] the numerical analysis of the effect of parameters on the periodic relative motion was conducted, and the method of non-negative polynomials was used to obtain a finite description of admissible periodic trajectories within a given region. Then, Arantes et al. [15] introduced a novel description of space-restricted periodic

*PhD Candidate, Department of Aerospace Science and Technology, Via La Masa 34, 20156 Milano, Italy, Email: chuncheng.zhao@polimi.it, Corresponding Author.
†Assistant Professor, Department of Aerospace Science and Technology, Via La Masa 34, 20156 Milano, Italy, Email: michele.maestrini@polimi.it.
‡Associate Professor, Department of Aerospace Science and Technology, Via La Masa 34, 20156 Milano, Italy, Email: pierluigi.dilizia@polimi.it, AIAA Member.

trajectories using polynomial inequalities, which is simpler and more numerically efficient. Subsequently, a global stability controller with a three-impulse sequence was designed in Ref. [16] according to the novel admissible trajectory set. Recently, Sanchez et al. [17] proposed an event-triggered controller to perform hovering with impulsive maneuvers. As technology evolves, the requirements and operating constraints imposed on the design of space missions are also constantly tightened. Recent research is shifting towards the adoption of small or lightweight satellites such as Cubesats [18], thanks to their low energy consumption, easy mass production, and cost-effectiveness. On the other hand, these small platforms are limited by their reduced resources in terms of computation, power, and actuation capabilities. As a consequence, the ability to perform attitude and orbital control maneuvers is severely constrained [19]. In addition, the efficiency of autonomous guidance and control algorithms needs to be constantly taken into account while designing the algorithms for these satellites due to the limited computing resources available onboard [6, 20].

In this paper, the control design is based on the search of constrained periodic orbits, and it aims at providing autonomous guidance for a satellite equipped with a low-thrust engine to carry out an inspection mission. However, the application of unconstrained optimal control laws presents some difficulties in terms of implementation on platforms with limited actuation capacity. For example, the direction of the thrust in unconstrained cases may vary rapidly. As a consequence, the required control profile would be unfeasible for a spacecraft equipped with few engines and a limited slew rate. This issue may be mitigated by constraining the input to lie in a specific direction. Indeed, this work introduces an operational constraint on the thrust direction during the transfer by assuming that the satellite is equipped with two opposite thrusters that allow it to perform maneuvers only in the tangential direction [21]. The control purpose is to reach an optimal target point on a pre-designed target periodic orbit while maximizing the duration of the free drift relative motion inside the desired hovering region and minimizing the cost of the transfer. To perform this feat, first, an energy-optimal control problem is solved. The solution to this problem is available in a semi-analytical way, which makes it suitable for onboard execution on small satellites [22]. Nonetheless, the control profiles retrieved by such guidance laws are modulated and therefore they may not be realizable on a simple engine that is only capable of being switched on or off. Subsequently, using this control as an initial guess, a fast semi-analytical method can be devised to convert the control profile to a bang-bang structure that satisfies the conditions of a fuel-optimal control problem. This feat can be achieved thanks to the assumption of tangential-only thrust. To conclude, a strategy for long-term hovering obtained by concatenating phases of free orbital drift and controlled trajectories is proposed.

This paper is organized as follows. Sec. II gives the dynamical models used to obtain the periodicity condition of the relative orbits and to design the solution of the optimal control problems. Subsequently, Sec. III gives an analytical method to solve the energy-optimal control problem and presents the semi-analytical method to deal with the fuel-optimal control problem. Then, Sec. IV presents the building blocks necessary for the selection of target points for the controller during the long-term hovering strategy. Finally, Sec. V concludes the paper and discusses the limitations of the current approach.

II. Dynamical models

This section illustrates the dynamical models used during the control design and the simulation stage. Specifically, a dynamical system expressed in the inertial Cartesian frame is used to design the optimal control. Conversely, a relative dynamical model is adopted to design constrained periodic relative orbits.

A. Inertial dynamic

In this paper, the passive spacecraft which is the object of proximity operations will be referred to as the "leader". The active spacecraft that is capable of performing maneuvers will instead be called the "follower". As shown in Fig.1, the LVLH frame which is centered on the mass center of the leader S_l is denoted by $\{S_l, \boldsymbol{i}, \boldsymbol{j}, \boldsymbol{k}\}$. The Earth-Centered Inertial (ECI) frame is denoted by $\{O, \boldsymbol{I}, \boldsymbol{J}, \boldsymbol{K}\}$. It is noted that $\boldsymbol{k}$ is the radial vector positive toward the center of the Earth O, $\boldsymbol{j}$ is the cross-track vector opposite to the orbit angular momentum, and $\boldsymbol{i}$ is the in-track vector satisfying the right-handed rule. The relative position $\boldsymbol{\rho}$ of the follower S_f is expressed in the LVLH frame. Whereas $\boldsymbol{r}_f$ and $\boldsymbol{r}_l$ represent the inertial position of the two spacecrafts in the ECI frame.

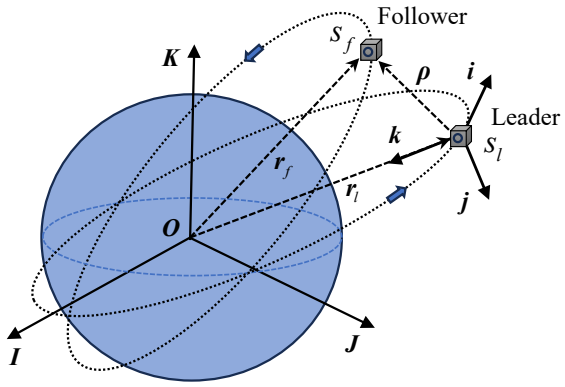

Fig. 1 Inertial Earth-centered frame and LVLH frame.

The control acceleration term is added directly to the formulation of the inertial dynamics for the follower since this model is more convenient to include orbital perturbations and it makes it possible to retrieve analytical solutions of the energy-optimal control problem. Based on the assumption of Keplerian motion, the inertial dynamics with J_2 and atmospheric drag perturbations can be written in the ECI frame as,

$$\begin{cases} \boldsymbol{r} = \dot{\boldsymbol{v}} \\ \dot{\boldsymbol{v}} = -\frac{\mu}{r^3}\boldsymbol{r} + \boldsymbol{a}_{\mathrm{J}_2} + \boldsymbol{a}_{\mathrm{drag}} + \boldsymbol{a}_c \end{cases} \tag{1}$$

where μ is Earth's gravitational constant. Throughout this paper, the vector [$\boldsymbol{r}$; $\boldsymbol{v}$] refers to the inertial state of the follower omitting the subscript f. $\boldsymbol{a}_{\mathrm{J}_2}$, $\boldsymbol{a}_{\mathrm{drag}}$, and $\boldsymbol{a}_c$ represent J_2 perturbation, atmospheric drag, and control

accelerations respectively. In this paper, it was assumed that the variation of mass of the maneuvering spacecraft is negligible, which is typical for proximity operations. This assumption allows us to directly deal with control accelerations in the formulation of the optimal control problems, and it makes it possible to remove the variational equation of the mass from the state. The J_2 and atmospheric drag perturbations are considered during the propagation of the disturbed relative motion, yet they are not included in the design of optimal control in this paper. Consequently, these two perturbed terms are omitted during the derivation of the optimal control problem carried out in Sec. III. In addition, a model from [23, 24] is used to simulate the realistic non-linear disturbed relative motion for the simulations carried out in Sec.III and IV.

B. Relative dynamics

This section introduces a simplified relative dynamical model which will be used to design target periodic orbits. Under the assumption of Keplerian motion and considering that the distance between the leader and the follower spacecrafts is much smaller than the distance between the leader and the Earth's center (i.e., $\|\boldsymbol{r}_l\| \gg \|\boldsymbol{\rho}\|$), the relative dynamics expressed in the LVLH frame can be described as a state-space representation using linearized Tschauner–Hempel equations [25],

$$\dot{\boldsymbol{X}}(t) = \boldsymbol{A}(t)\boldsymbol{X}(t) \tag{2}$$

where the state vector $\boldsymbol{X}$ represents the relative position and velocity, $\boldsymbol{X}(t) = [x(t); y(t); z(t); \dot{x}(t); \dot{y}(t); \dot{z}(t)]$. To obtain a closed-form solution of Eq. 2, a similarity transformation from independent variable time t to the true anomaly ν is applied as,

$$\tilde{\boldsymbol{X}}(\nu) = \begin{bmatrix} \rho_\nu \boldsymbol{I}_3 & \boldsymbol{0}_3 \\ -e\sin\nu \boldsymbol{I}_3 & \sqrt{\frac{a^3(1-e^2)^3}{\mu\rho_\nu^2}}\boldsymbol{I}_3 \end{bmatrix} \boldsymbol{X}(t) \tag{3}$$

where the variables a and e are the leader's orbit semi-major axis and eccentricity with $\rho_\nu = (1 + e\cos\nu)$. The symbols $\boldsymbol{I}_3$ and $\boldsymbol{0}_3$ represent the 3×3 identity and zero matrices respectively. Based on Eq.3 Yamanaka and Ankersen [26] formulated a state-space model in the variable ν for which an analytical state transition matrix could be obtained. This state transition matrix can then be directly used for the propagation of relative motion from an initial state $\tilde{\boldsymbol{X}}(\nu_0)$. The equations of relative position can then be expressed as [13]:

$$\begin{aligned}
\tilde{x}(\nu) &= d_1(\nu_0)(2 + ec_\nu)s_\nu - d_2(\nu_0)(2 + ec_\nu)c_\nu + d_3(\nu_0) + 3(1 + ec_\nu)^2 d_0(\nu_0)J_{\nu_0}(\nu) \\
\tilde{y}(\nu) &= d_4(\nu_0)c_\nu + d_5(\nu_0)s_\nu \\
\tilde{z}(\nu) &= d_1(\nu_0)(1 + ec_\nu)c_\nu + d_2(\nu_0)(1 + ec_\nu)s_\nu - 3es_\nu(1 + ec_\nu)d_0(\nu_0)J_{\nu_0}(\nu) + 2d_0(\nu_0)
\end{aligned} \tag{4}$$

where $s_\nu = \sin\nu$ and $c_\nu = \cos\nu$. $J_{\nu_0}(\nu)$ is an integral term and the specific expression can be found in Ref. [16]. The parameters $d_i(\nu_0)$ with $i \in [0,1,2,3,4,5]$ are factored terms that only depend on ν_0. Inspired by Eq. 4, the concept of the vector of parameters $\boldsymbol{D}(\nu) = [d_0(\nu), d_1(\nu), d_2(\nu), d_3(\nu), d_4(\nu), d_5(\nu)]$ was proposed in [14]. This set of parameters satisfies,

$$\boldsymbol{D}(\nu) = \underbrace{\begin{bmatrix} 0 & 0 & -\frac{3ec_\nu+e^2+2}{e^2-1} & \frac{\rho_\nu^2}{e^2-1} & 0 & -\frac{es_\nu\rho_\nu}{e^2-1} \\ 0 & 0 & \frac{3(e+c_\nu)}{e^2-1} & -\frac{2c_\nu+ec_\nu^2+e}{e^2-1} & 0 & \frac{s_\nu\rho_\nu}{e^2-1} \\ 0 & 0 & \frac{3s_\nu(\rho_\nu+e^2)}{\rho_\nu(e^2-1)} & -\frac{s_\nu(1+\rho_\nu)}{e^2-1} & 0 & \frac{2e-c_\nu\rho_\nu}{e^2-1} \\ 1 & 0 & -\frac{3es_\nu(1+\rho_\nu)}{\rho_\nu(e^2-1)} & \frac{es_\nu(1+\rho_\nu)}{e^2-1} & 0 & \frac{ec_\nu\rho_\nu-2}{e^2-1} \\ 0 & c_\nu & 0 & 0 & -s_\nu & 0 \\ 0 & s_\nu & 0 & 0 & c_\nu & 0 \end{bmatrix}}_{\boldsymbol{C}(\nu)} \tilde{\boldsymbol{X}}(\nu) \tag{5}$$

Combining Eq. 3 and Eq. 5, we can obtain

$$\boldsymbol{D}(\nu) = \boldsymbol{C}(\nu) \begin{bmatrix} (1+ec_\nu)\boldsymbol{I}_3 & \boldsymbol{0}_3 \\ -es_\nu\boldsymbol{I}_3 & \sqrt{\frac{a^3(1-e^2)^3}{\mu(1+ec_\nu)^2}}\boldsymbol{I}_3 \end{bmatrix} \boldsymbol{X}(t) \tag{6}$$

Eq. 6 gives a direct transformation between relative states and the vector of parameters at the time instant t (or equivalent ν), which will be useful in the fuel-optimal control problem. Moreover, by looking at Eq. 4, it can be noticed that the relative motion in the out-of-plane direction is naturally periodic. Conversely, to obtain periodic in-plane motion the parameter d_0 must be set to 0, which eliminates the effect of the drifting term $J_{\nu_0}(\nu)$. Therefore, the periodicity condition at the initial moment t_0 or ν_0 is written as,

$$d_0(\nu_0) = es_{\nu_0}x(t_0) - \sqrt{\frac{a^3(1-e^2)^3}{\mu(1+ec_{\nu_0})^2}}\dot{x}(t_0) + \frac{2+3ec_{\nu_0}+e^2(1-s_{\nu_0}^2)}{1+ec_{\nu_0}}z(t_0) + \frac{es_{\nu_0}}{1+ec_{\nu_0}}\sqrt{\frac{a^3(1-e^2)^3}{\mu(1+ec_{\nu_0})^2}}\dot{z}(t_0) = 0 \tag{7}$$

From Eq. 7 it is also possible to observe that the periodicity condition is only related to in-plane states. In addition, the vector of parameters $\boldsymbol{D}$ will be constant for a periodic orbit [14]. Hence, by introducing the periodicity condition into

Eq. 4 and by substituting it into Eq. 3, an analytical solution of periodic orbit can be retrieved directly [12, 13].

$$\begin{aligned} \tilde{x}(\nu) &= (2+es_\nu)(d_1 s_\nu - d_2 c_\nu) + d_3 \qquad & x(\mathrm{t}) &= \left((2+ec_\nu)\sqrt{d_1^2+d_2^2}\sin\left(\nu - \arctan\tfrac{d_2}{d_1}\right) + d_3\right)/(1+ec_\nu) \\ \tilde{y}(\nu) &= d_4 c_\nu + d_5 s_\nu \qquad \Rightarrow & y(t) &= \sqrt{d_4^2+d_5^2}\sin\left(\nu + \arctan\tfrac{d_4}{d_5}\right)/(1+ec_\nu) \\ \tilde{z}(\nu) &= (1+es_\nu)(d_1 c_\nu + d_2 s_\nu) & z(t) &= \sqrt{d_1^2+d_2^2}\sin\left(\nu + \arctan\tfrac{d_1}{d_2}\right) \end{aligned} \tag{8}$$

In this formulation, the dependency from ν_0 has been omitted to simplify the notation.

III. Low-thrust optimal control

This section is dedicated to the mathematical developments necessary to retrieve the optimal control solutions of the hovering problem. First, the mathematical derivation of an analytical method for the design of low-thrust energy-optimal control will be presented, which is based on the seminal work of De Vittori et al. [22]. Then, Sect. III.B will present a semi-analytical solution to the fuel-optimal control problem based on [27, 28]. To avoid directly dealing with the solution of this problem, the control law derived from the solution of the energy optimal problem will be used to provide an initial guess that will speed up its convergence.

A. Energy-optimal control

To be able to retrieve an analytic solution, the control design will disregard the effects of the drag and Earth's nonhomogeneous gravitational field. As mentioned in the introduction, the control thrust is provided by two engines firing in opposite directions, which are restricted to operate exclusively in the tangential direction. This constraint serves a dual purpose. Firstly, it mitigates the need for fast attitude slewing maneuvers that may be required to track an unconstrained control profile. Secondly, it facilitates the formulation of the fuel-optimal control problem through the utilization of a semi-analytic technique as illustrated in Sec. III.B. Hence, the control acceleration vector is aligned with $\boldsymbol{v}/v$. Then, by inserting this constraint into the dynamics,

$$\begin{cases} \dot{\boldsymbol{r}} = \boldsymbol{v} \\ \dot{\boldsymbol{v}} = -\frac{\mu}{r^3}\boldsymbol{r} + a_t \frac{\boldsymbol{v}}{v} \end{cases} \qquad \text{Initial Conditions:} \begin{cases} \boldsymbol{r}(t_0) = \boldsymbol{r}_0 \\ \boldsymbol{v}(t_0) = \boldsymbol{v}_0 \end{cases} \tag{9}$$

Here $\boldsymbol{a}_c = a_t \boldsymbol{v}/v$, and a_t is the magnitude of tangential control acceleration. Since the tangential thrust is assumed to be applied in the orbital plane of the follower, the out-of-plane target relative state (the $\boldsymbol{j}$ direction of LVLH) can not be reached. Therefore, the distance between the controlled final relative states and target relative states is introduced as a terminal cost to approach the target point as close as possible.

$$\varphi(\boldsymbol{X}_f) = \left(\boldsymbol{X}_f - \boldsymbol{X}_t\right)^{\mathrm{T}} Q \left(\boldsymbol{X}_f - \boldsymbol{X}_t\right), Q = diag(q_1, q_2, q_3, q_4, q_5, q_6). \tag{10}$$

Here $\boldsymbol{X}_f$ is the vector of controlled final relative states, $\boldsymbol{X}_t$ is the vector of target relative states, and Q is a positive definite weight matrix. On the other hand, the tangential thrust does not prevent the periodicity condition of terminal states in Eq. 7 to be included as a final state constraint $\psi(\boldsymbol{X}_f) = d_0 = 0$. Under these assumptions, the augmented cost function with a fixed final time t_f can be expressed as,

$$J = \varphi(\boldsymbol{X}_f) + \int_{t_0}^{t_f} \left(\frac{1}{2} a_t^2 + \boldsymbol{\lambda}_r^{\mathrm{T}} \left(\boldsymbol{v} - \dot{\boldsymbol{r}} \right) + \boldsymbol{\lambda}_v^{\mathrm{T}} \left(-\frac{\mu}{r^3} \boldsymbol{r} + a_t \frac{\boldsymbol{v}}{v} - \dot{\boldsymbol{v}} \right) \right) dt \tag{11}$$

Consequently, the Hamiltonian is,

$$H = \frac{1}{2} a_t^2 + \boldsymbol{\lambda}_r^{\mathrm{T}} \boldsymbol{v} + \boldsymbol{\lambda}_v^{\mathrm{T}} (-\frac{\mu}{r^3} \boldsymbol{r} + a_t \frac{\boldsymbol{v}}{v}) \tag{12}$$

where the only controllable variable is a_t. From Pontryagin's minimum principle, the optimal control law minimizing the Hamiltonian yields,

$$a_t^* = -\boldsymbol{\lambda}_v \cdot \frac{\boldsymbol{v}}{v} \tag{13}$$

Then, this optimal control problem can be solved as [29],

$$\begin{cases} \dot{\boldsymbol{r}} = \boldsymbol{v} \\ \dot{\boldsymbol{v}} = -\frac{\mu}{r^3} \boldsymbol{r} - \left(\boldsymbol{\lambda}_v \cdot \frac{\boldsymbol{v}}{v} \right) \frac{\boldsymbol{v}}{v} \\ \dot{\boldsymbol{\lambda}}_r = \frac{\mu}{r^3} \boldsymbol{\lambda}_v - \frac{3\mu \boldsymbol{r} \cdot \boldsymbol{\lambda}_v}{r^5} \boldsymbol{r} \\ \dot{\boldsymbol{\lambda}}_v = -\boldsymbol{\lambda}_r + \frac{\boldsymbol{\lambda}_v \cdot \boldsymbol{v}}{v^2} \left(\boldsymbol{\lambda}_v - \frac{\boldsymbol{\lambda}_v \cdot \boldsymbol{v}}{v^2} \boldsymbol{v} \right) \end{cases} \quad \text{Boundary Conditions:} \begin{cases} \boldsymbol{r}(t_0) = \boldsymbol{r}_0 \\ \boldsymbol{v}(t_0) = \boldsymbol{v}_0 \\ \boldsymbol{\lambda}_r(t_f) = \frac{\partial (\varphi(\boldsymbol{X}_f) + \kappa \psi(\boldsymbol{X}_f))}{\partial \boldsymbol{r}_f} \\ \boldsymbol{\lambda}_v(t_f) = \frac{\partial (\varphi(\boldsymbol{X}_f) + \kappa \psi(\boldsymbol{X}_f))}{\partial \boldsymbol{v}_f} \end{cases} \tag{14}$$

In this equation, κ is an additional unknown Lagrange multiplier corresponding to the final state constraint. Reference [29] provides a thorough overview of how this coefficients is included in the formulation of the optimal control problem. This two-point-boundary-value problem can be transformed into an Initial Value Problem (IVP) aiming to find the initial costates $(\boldsymbol{\lambda}_{r_0}, \boldsymbol{\lambda}_{v_0})$. To this aim, Eqs. 14 are linearized around the nominal uncontrolled dynamics, and the State Transition Matrix (STM) $\boldsymbol{\Phi}$ is employed to analytically propagate variations of initial states and costates within the given time frame. This assumption allows us to integrate the Keplerian dynamics and retrieve the STM only once for the desired time window, which significantly reduces computational time. The STM can be computed from the following set of ODEs,

$$\dot{\boldsymbol{\Phi}}(t, t_0) = \boldsymbol{A}(t) \boldsymbol{\Phi}(t, t_0) \qquad \boldsymbol{\Phi}(t_0, t_0) = \boldsymbol{I}_{n \times n} \tag{15}$$

where $\boldsymbol{A}$ is the Jacobian of the dynamics system expressed in Eq. 14 and evaluated on the nominal Keplerian orbit as:

$$\boldsymbol{A} = \begin{bmatrix} \mathbf{0}_{3\times3} & \boldsymbol{I}_{3\times3} & \mathbf{0}_{3\times3} & \mathbf{0}_{3\times3} \\ -\boldsymbol{A}_{34} & \mathbf{0}_{3\times3} & \mathbf{0}_{3\times3} & \boldsymbol{A}_{24} \\ \mathbf{0}_{3\times3} & \mathbf{0}_{3\times3} & \mathbf{0}_{3\times3} & \boldsymbol{A}_{34} \\ \mathbf{0}_{3\times3} & \mathbf{0}_{3\times3} & -\boldsymbol{I}_{3\times3} & \mathbf{0}_{3\times3} \end{bmatrix}, \; \boldsymbol{A}_{24} = -\left[\frac{\boldsymbol{v}}{v}\left(\frac{\boldsymbol{v}}{v}\right)^{\mathrm{T}}\right], \boldsymbol{A}_{34} = \frac{\mu}{r_n^3}\boldsymbol{I}_{3\times3} - \frac{3\mu}{r_n^5}\begin{bmatrix} {r_{nx}}^2 & r_{nx}r_{ny} & r_{nx}r_{nz} \\ r_{nx}r_{ny} & {r_{ny}}^2 & r_{ny}r_{nz} \\ r_{nx}r_{nz} & r_{ny}r_{nz} & {r_{nz}}^2 \end{bmatrix}. \quad (16)$$

Here $\boldsymbol{r}_n = [r_{nx}; r_{ny}; r_{nz}]$ represents the inertial position of nominal trajectory. Next, the variations of initial states are linearly mapped into variations of final states thanks to the STM,

$$\begin{bmatrix} \delta\boldsymbol{r}_f \\ \delta\boldsymbol{v}_f \\ \delta\boldsymbol{\lambda}_{rf} \\ \delta\boldsymbol{\lambda}_{vf} \end{bmatrix} = \begin{bmatrix} \boldsymbol{\Phi}_{11} & \boldsymbol{\Phi}_{12} & \boldsymbol{\Phi}_{13} & \boldsymbol{\Phi}_{14} \\ \boldsymbol{\Phi}_{21} & \boldsymbol{\Phi}_{22} & \boldsymbol{\Phi}_{23} & \boldsymbol{\Phi}_{24} \\ \boldsymbol{\Phi}_{31} & \boldsymbol{\Phi}_{32} & \boldsymbol{\Phi}_{33} & \boldsymbol{\Phi}_{34} \\ \boldsymbol{\Phi}_{41} & \boldsymbol{\Phi}_{42} & \boldsymbol{\Phi}_{43} & \boldsymbol{\Phi}_{44} \end{bmatrix} \begin{bmatrix} \delta\boldsymbol{r}_0 \\ \delta\boldsymbol{v}_0 \\ \delta\boldsymbol{\lambda}_{r0} \\ \delta\boldsymbol{\lambda}_{v0} \end{bmatrix} \quad (17)$$

Since the initial states are fixed, $\delta\boldsymbol{r}_0 = 0$ and $\delta\boldsymbol{v}_0 = 0$, and the previous expression can be simplified. Moreover, since the costates are zero on the nominal trajectory, then $\delta\boldsymbol{\lambda} = \boldsymbol{\lambda}$ at all times. Meanwhile, the variations of the final states are imposed given that specific target position and velocity are required to achieve the desired target state on a relative periodic orbit: $\delta\boldsymbol{r}_f = \boldsymbol{r}_f - \boldsymbol{r}_p$, $\delta\boldsymbol{v}_f = \boldsymbol{v}_f - \boldsymbol{v}_p$. Here $\boldsymbol{r}_p$ and $\boldsymbol{v}_p$ represent the final nominal states obtained from the propagation of simple Keplerian motion. As a consequence, the IVP can be solved by a system of 13 equations with 13 unknowns (i.e., $[\boldsymbol{r}_f, \boldsymbol{v}_f, \boldsymbol{\lambda}_{r0}, \boldsymbol{\lambda}_{v0}, \kappa]$) which is formulated by introducing these assumptions in Eq. 17 and by adding the boundary conditions presented in Eq.14.

$$\begin{cases} \boldsymbol{r}_f - \boldsymbol{r}_p - \boldsymbol{\Phi}_{13}\boldsymbol{\lambda}_{r0} - \boldsymbol{\Phi}_{14}\boldsymbol{\lambda}_{v0} = 0 \\ \boldsymbol{v}_f - \boldsymbol{v}_p - \boldsymbol{\Phi}_{23}\boldsymbol{\lambda}_{r0} - \boldsymbol{\Phi}_{24}\boldsymbol{\lambda}_{v0} = 0 \\ \frac{\partial(\varphi(\boldsymbol{X}_f) + \kappa\psi(\boldsymbol{X}_f))}{\partial\boldsymbol{r}_f} - \boldsymbol{\Phi}_{33}\boldsymbol{\lambda}_{r0} - \boldsymbol{\Phi}_{34}\boldsymbol{\lambda}_{v0} = 0 \\ \frac{\partial(\varphi(\boldsymbol{X}_f) + \kappa\psi(\boldsymbol{X}_f))}{\partial\boldsymbol{v}_f} - \boldsymbol{\Phi}_{43}\boldsymbol{\lambda}_{r0} - \boldsymbol{\Phi}_{44}\boldsymbol{\lambda}_{v0} = 0 \\ \psi(\boldsymbol{X}_f) = 0 \end{cases} \quad (18)$$

B. Fuel-optimal control

The fuel-optimal control problem can leverage the results of the energy-optimal control problem to help convergence and an outline of the solution is provided in Fig. 2.

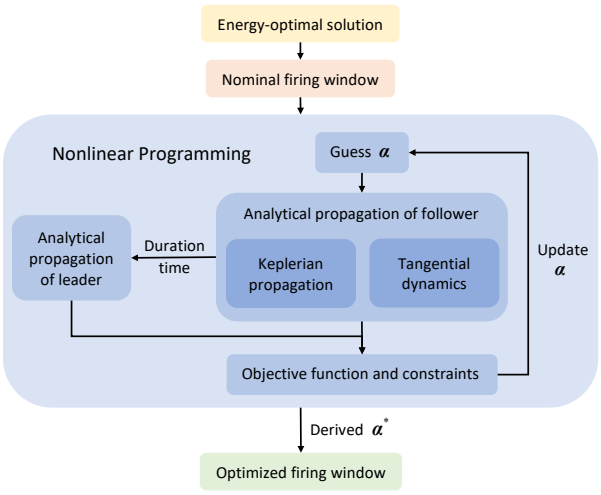

Fig. 2 Proposed procedure for the solution of the fuel-optimal control problem.

First, an initial guess of firing windows (i.e., those parts of the trajectory that have full thrust) is acquired according to a procedure devised in [22]. This method starts by determining the equivalent burning time of the energy-optimal control (i.e., a_t) that is estimated based on the definition of a maximum acceleration $a_{\max}$ for the fuel-optimal control problem. Then, the bisection algorithm determines a threshold value of acceleration a_{th} so that the initial guess for the firing windows matches this total burning time. Indeed, a_{th} is used to determine when thrusters are switched on (i.e., $|a_t| \geq a_{\text{th}}$). Fig.3(a) provides a schematic diagram of how the Nominal Firing Windows can be obtained.

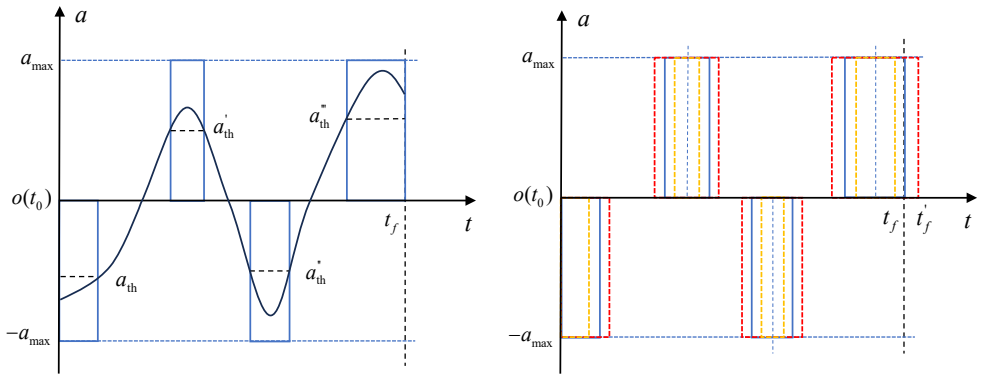

(a) Determination of the nominal firing window

(b) Expansion (red) and reduction (yellow) of the firing windows

Fig. 3 Overview of the firing window determination process from the initial guess (a) to the final one obtained after optimization (b).

After having obtained an initial guess for the optimization problem, a Non-Linear Programming (NLP) problem is set up to find the optimal bang-bang thrust profile by adjusting the firing windows so that some constraining conditions are satisfied. The first constraint imposed in the NLP is that the centers of the thrusting arcs are fixed. Then, the amplitude

of each firing window can be expanded or shortened by multiplying them by their associated factors α_k, $k = 1, 2, ..., L$, where L is the number of firing windows as illustrated in Fig.3(b). Additionally, a constraint is added to verify that subsequent thrusting arcs do not intersect. As a consequence, the number of firing windows cannot be increased, but it can be reduced if any of the α factors decreases to zero. Moreover, it must be noticed that the final time provided by the solution of the energy-optimal control problem barely constitutes an initial guess for the final time retrieved by the solution of the fuel-optimal control problem. If the final firing window is enlarged past the nominal control time, then the control time is extended to completely include the last maneuver. The objective of this NLP problem is to find an optimal vector of factors $\boldsymbol{\alpha}^*$ that minimizes a custom objective function under the above-mentioned constraints. The objective function selected for the fuel-optimal problem combines both the final distance to a target point and the total fuel cost (i.e., represented by the total burning time) as:

$$F(\alpha) = \eta[\Delta t_1(\alpha_1) + \Delta t_2(\alpha_2) + \cdots + \Delta t_L(\alpha_L)] + \varphi(\mathbf{X}_f) \tag{19}$$

where η is a weight factor to balance the contribution to the fuel cost.

When a guess structure of firing windows is available, the trajectory is analytically propagated with an asymptotic method with constant tangential acceleration [27]. The adoption of analytical propagations inside the optimization problem provides a significant boost to the computational time required for the solution of the fuel-optimal control problem. To apply Bombardelli's method for analytical propagation of the accelerated dynamics, the nominal firing windows are converted from time ranges to true anomaly ranges as shown in [30]. The complete process for the solution of the fuel-optimal control problem is summarized in Algorithm 1.

C. Numerical validation

Some simulations are conducted to demonstrate the efficacy of the control methods proposed in this section. The Simulink model of Ref. [24] is adopted as a ground truth dynamical model which is based on the nonlinear Gauss variational equations including Earth J_2 oblateness effect and atmospheric drag as perturbations sources. The parameters used for simulating are given in Table 1. In this paper, the two spacecrafts are considered to be similar, so ballistic coefficients, that is $B = \frac{SC_D}{m}$, are set as $B_l = 150.30\text{kg/m}^2$ and $B_f = 153.40\text{kg/m}^2$, respectively. The values of the follower have been directly taken from [24]. This ballistic coefficient represents an average value between the ISS and the ATV as taken from [17]. The initial classical orbital elements of the leader are a perigee altitude of $P = 450\text{km}$, an eccentricity of $e = 0.1$, and an inclination of $i = 30^\circ$ while the rest of the elements are set to 0 [17, 24].

The hovering zone is defined as a cube along the positive $\boldsymbol{i}$ direction of the LVLH frame and it can be defined by upper (overline) and lower (underline) bounds, $\{\underline{x} = 40\text{m}, \overline{x} = 100\text{m}, \underline{y} = -30\text{m}, \overline{y} = 30\text{m}, \underline{z} = -30\text{m}, \overline{z} = 30\text{m}\}$ [16, 17]. Finally, the relative state is set to $[80\text{m}; 10\text{m}; -5\text{m}; -0.0112\text{m/s}; 0\text{m/s}; -0.0100\text{m/s}]$ with a corresponding vector of

Algorithm 1 NLP for the solution of the fuel-optimal control problem.

Input: Earth's gravitational constant: μ. Maximum acceleration: $a_{\max}$. Initial inertial state of the follower: $\boldsymbol{I}_0$. Initial inertial states of leader: $\boldsymbol{I}_{l0}$. Nominal true anomaly interval of firing-on windows: $\Delta\nu_k^{\text{on}}$. Vector containing nominal true anomaly sequence of accelerated and non-accelerated dynamics: $\boldsymbol{\nu}^{\text{seq}}$.

Output: Optimized firing window.

Set all the values of the vector of factors $\boldsymbol{\alpha}$ to 1 to preserve the input nominal firing windows.
while Stopping criterion not met **do**
  Initialize the Flag to label the number of firing windows: $k = 1$;
  Total propagation time initialization: $t_p = 0$;
  Compute the total number of firing windows: $L = length(\Delta\nu_k^{\text{on}})$;
  for the index $j = 1 : 2 : length(\boldsymbol{\nu}^{\text{seq}})$ **do**
    if thrusters at $\nu^{\text{seq}}(j, j+1)$ are on **then**
      Propagate the accelerated states with Bombardelli's method:
      $[\boldsymbol{I}_f, t_{\text{on}}] = BombardelliPropagation(\boldsymbol{I}_0, \alpha_k \Delta\nu_k^{\text{on}}, a_{\max}, \mu)$;
      Update the initial states: $\boldsymbol{I}_0 = \boldsymbol{I}_f$;
      Update the propagation time: $t_p = t_p + t_{\text{on}}$;
      Update the Flag of firing-on window: $k = k + 1$;
    else if thrusters at $\boldsymbol{\nu}^{\text{seq}}(j, j+1)$ are off **then**
      Calculate initial true anomaly th_0 of non-accelerated windows from inertial states $\boldsymbol{I}_0$;
      Calculate true anomaly range $\Delta\nu^{\text{off}}$ of coasting windows:
      if thrusters are off at the end arc **then**
        if $k \leq L$ **then**
          $\Delta\nu^{\text{off}} = \boldsymbol{\nu}^{\text{seq}}(j+1) - \Delta\nu_k^{\text{on}}(\alpha_k - 1)/2 - th_0$;
        else
          $\Delta\nu^{\text{off}} = \boldsymbol{\nu}^{\text{seq}}(j+1) - th_0$;
        end if
      else if thrusters are on at the end arc **then**
        if $k < L$ **then**
          $\Delta\nu^{\text{off}} = \boldsymbol{\nu}^{\text{seq}}(j+1) - \Delta\nu_k^{\text{on}}(\alpha_k - 1)/2 - th_0$;
        else
          $\Delta\nu^{\text{off}} = \boldsymbol{\nu}^{\text{seq}}(j+1) - \Delta\nu_k^{\text{on}}(\alpha_k - 1) - th_0$;
        end if
      end if
      Convert true anomaly range $\Delta\nu^{\text{off}}$ to time range t_{off};
      Propagate the non-accelerated states with Keplerian dynamics:
      $\boldsymbol{I}_f = KeplerianPropagation(\boldsymbol{I}_0, \Delta\nu^{\text{off}}, \mu)$;
      Update the initial states: $\boldsymbol{I}_0 = \boldsymbol{I}_f$;
      Update the propagation time: $t_p = t_p + t_{\text{off}}$;
    end if
  end for
  Analytical propagation of final inertial states of leader: $\boldsymbol{I}_{lf} = AnalyticalSTM(\boldsymbol{I}_{l0}, t_p, \mu)$;
  Convert final inertial relative states $(\boldsymbol{I}_f - \boldsymbol{I}_{lf})$ to final relative states $\boldsymbol{X}_f$;
  Equality constraint: periodicity condition at $\boldsymbol{X}_f$;
  Inequality constraints: no-intersection of two firing-on windows;
  Cost function: $\eta[\Delta t_1(\alpha_1) + \Delta t_2(\alpha_2) + \cdots + \Delta t_L(\alpha_L)] + \varphi(\mathbf{X}_f)$.
  Adjust $\boldsymbol{\alpha}$ according to the optimizer (e.g., Matlab's fmincon).
end while

Table 1 Parameters of simulation

Parameters	Value
Gravitational parameter of Earth	$\mu = 3.986004 \times 10^5 \text{km}^3/\text{s}^2$
Radius of the Earth	$R_e = 6.378136 \times 10^3 \text{km}$
J_2 parameter	1.08263×10^{-3}
Ballistic coefficients	$B_l = 150.30 \text{kg}/\text{m}^2$,$B_f = 153.40 \text{kg}/\text{m}^2$
Initial orbital elements of leader	$P = 450\text{km}$, $e = 0.1$, $i = 30°$, $\Omega = 0$, $\omega = 0$, $\nu = 0$
Boundary values of hovering zone	$\underline{x} = 40\text{m}, \overline{x} = 100\text{m}, \underline{y} = -30\text{m}, \overline{y} = 30\text{m}, \underline{z} = -30\text{m}, \overline{z} = 30\text{m}$

parameters $\boldsymbol{D} = [0; -5; -8.521; 70.106; 11; 0]$. This selection ensures that the relative orbit is periodic according to Eq. 7 and it lies inside the hovering zone. Fig.4 shows the results of the propagation from these initial conditions until the disturbed trajectory arrives at the boundary of the hovering region. Once the disturbed motion reaches this boundary, the fuel-optimal control is adopted to bring the follower back to a relative periodic orbit that lies inside the admissible region.

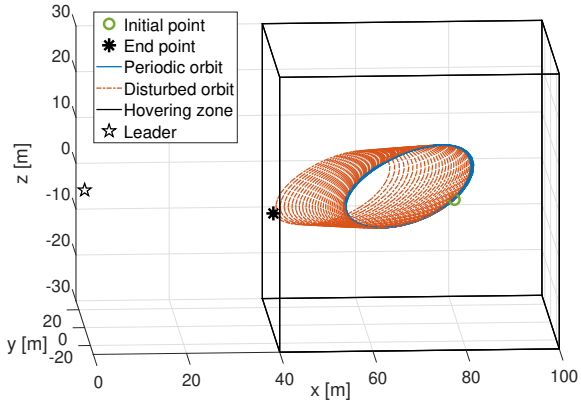

Fig. 4 Simulation of disturbed motion.

For this preliminary validation, the initial relative orbit is adopted as the target of the control. By further setting the control time to 1 orbital period of the leader, the target point is also fixed. The details about the design of an optimal target point will be discussed in Sec. IV. Next, both energy-optimal and fuel-optimal control problems are solved and simulated with unperturbed dynamics to demonstrate the ability to reach the desired conditions with the designed controls. In subsequent analyses, the perturbations will be added and their effect during control will be assessed.

Fig.5 shows an example of the solution achieved by the proposed methods. The adopted weight matrix for the energy-optimal problem is $Q = diag(1, 1, 1, 100, 100, 100)$, and the maximum acceleration is set as $a_{\max} = 3\times10^{-6}\text{m}/\text{s}^2$ [22, 28]. In addition, the weight factor η is set to 5 and it is kept unchanged for all following analyses. It is visually evident from Fig.5(a) and Fig. 5(b) that the tangential control designed by the solution of the energy-optimal control problem ends at a final point which has an error in the y state with respect to the target point. As mentioned during the

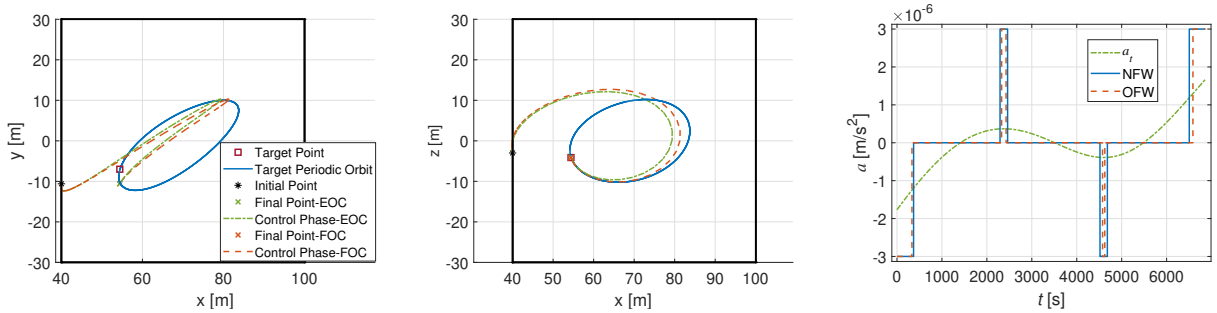

(a) Control phase in x-y plane (b) Control phase in x-z plane (c) Control profile

Fig. 5 Comparison of tangential energy-optimal control (EOC) and fuel-optimal control (FOC).

controller design, this behavior is expected. The thrust is indeed bound to be executed in the tangential direction of the follower. However, given the small magnitude of the relative states, the leader and follower exhibit very similar orbital elements. This results in a control authority that is approximately exerted in the $\boldsymbol{i}$-$\boldsymbol{k}$ plane of the LVLH frame of the leader. As a consequence, the out-of-plane component cannot be fully controlled. Moreover, the solution of the fuel-optimal control problem shows small in-plane state errors with respect to the target point. As a consequence, the final periodic orbit obtained slightly differs from the targeted one both out-of-plane and in-plane as illustrated in Fig.9. In the next section, a remedy to this problem will be presented by incorporating the boundaries of the target periodic orbit into the NLP as additional inequality constraints. The explanation for this behavior is rooted in the fact that the centers of the firing arcs remain fixed during their optimization. This limitation narrows the search space for feasible solutions for the fuel-optimal problem. A possible solution to this problem was obtained in [19] by combining closed loop and open loop controls. Despite these small final errors, the trajectory achieved after control is still guaranteed to be periodic, thanks to Eq. 7, which is imposed as a final constraint in the NLP. Finally, the nominal firing windows (NFW) defined by the bisection method and their optimized version obtained by NLP (OFW) are shown in Fig.5(c).

IV. Long-term hovering control

The strategy to perform long-term hovering control is developed in this section. The key idea is to design and execute a control action every time the follower spacecraft exits the hovering region due to the presence of orbital perturbations. To do so, the operations are divided into two main phases: a drifting phase, also named as hovering phase, and a control phase. The former is defined as a phase of uncontrolled relative motion inside the hovering region. The latter is defined as the controlled phase that brings the spacecraft from the boundary of the hovering region to the desired optimal target point. These two phases together form one cycle: long-term hovering control can be achieved via the design of multiple consecutive cycles. The recomputation of target periodic orbits is necessary after each drift phase. Indeed, the parameters determining the shape of the periodic orbit may change based on the leader's orbit eccentricity, which is

influenced by orbital perturbations. Once a target orbit is selected, various target points on this orbit can be obtained by adjusting the control duration. Performance metrics such as fuel consumption and the duration of drifting phases can then guide the selection and evaluation of target periodic orbits and their corresponding optimal target points. This process aims to provide a target relative state for optimal control design in each cycle. The selection of target points that maximize the drift time between cycles is motivated by the need to limit the number of maneuvers required for a more extended mission. Reducing the number of maneuvers allows for longer operational phases. However, it's important to note that longer drift times may necessitate larger maneuvers to recover the trajectory. All these considerations will be taken into account in the following analyses. To better clarify the long-term hovering procedure, the cycle to conduct operations is presented in Fig. 6.

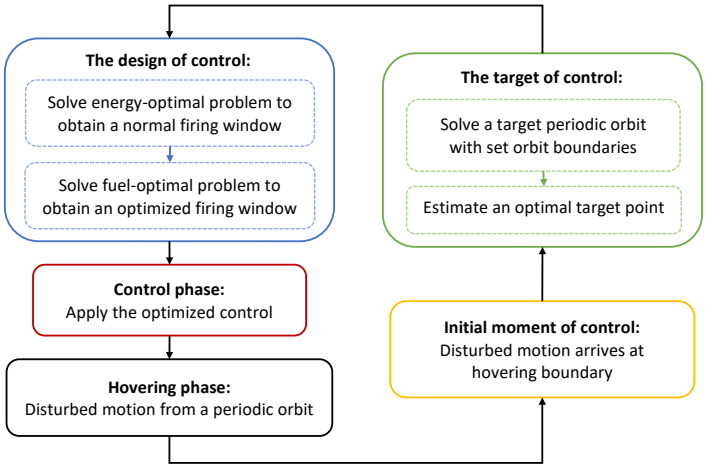

Fig. 6 Overview of the approach for long-term hovering.

A. Selection of the target periodic orbit

The first step before executing a control phase is to select a target periodic orbit. This subsection proposes a simple technique to find the vector of parameters $\boldsymbol{D}$ of a relative periodic orbit that lies inside a prescribed hovering zone based on polynomial inequalities description of space constraints [15, 23]. The description of the set of periodic orbits that satisfy the boundary constraints of a hovering zone is written as,

$$S_D = \left\{ \boldsymbol{D} \in R^6 | d_0 = 0, g_u\left(\boldsymbol{D}\right) \leq 0, \forall u \in \left[\underline{x}, \overline{x}, \underline{y}, \overline{y}, \underline{z}, \overline{z} \right] \right\} \tag{20}$$

where the functions $g_u\left(\boldsymbol{D}\right)$ are multivariate polynomials in d_1, d_2, d_3, d_4, and d_5. First, a multivariate polynomial in d_1, d_2, and d_3 is defined for the x state,

$$\hat{g}_x(d_1, d_2, d_3) = \sum_{r=0}^{6} \sum_{s=0}^{6} \sum_{w=0}^{4} \theta^{rsw}(e, x) d_1^r d_2^s d_3^w, \text{ and if } r + s + w > 6, \theta^{rsw} = 0. \tag{21}$$

In this expression, x could be substituted either with its upper or lower bound $\underline{x}$ and $\overline{x}$. $\theta^{rsw}(e,x)$ are the coefficients of the term $d_1^r d_2^s d_3^w$. This procedure can be done for all relative states, providing the following set of six polynomial inequalities,

$$g_{\underline{x}}(d_1,d_2,d_3) = \hat{g}_{\underline{x}} \leq 0, \tag{22}$$

$$g_{\overline{x}}(d_1,d_2,d_3) = \hat{g}_{\overline{x}} \leq 0, \tag{23}$$

$$g_{\underline{y}}(d_4,d_5) = (d_4 - e\underline{y})^2 + d_5^2 - \underline{y}^2 \leq 0, \tag{24}$$

$$g_{\overline{y}}(d_4,d_5) = (d_4 - e\overline{y})^2 + d_5^2 - \overline{y}^2 \leq 0, \tag{25}$$

$$g_{\underline{z}}(d_1,d_2) = d_1^2 + d_2^2 - \underline{z}^2 \leq 0, \tag{26}$$

$$g_{\overline{z}}(d_1,d_2) = d_1^2 + d_2^2 - \overline{z}^2 \leq 0, \tag{27}$$

The equations from 22 to 27 are conveniently used to determine whether a periodic orbit lies within the hovering zone defined by the boundary values. By solving these inequalities for their limit value (i.e., 0), it is possible to create a system of 6 equations in 6 unknowns, enabling the identification of the corresponding vector of parameters $\boldsymbol{D}$. First, it is possible to solve the equations related to the y boundary $[\underline{y}', \overline{y}']$ as it is decoupled from the x and z states,

$$\tilde{g}_{\underline{y}'}(d_4,d_5) = (d_4 - e\underline{y}')^2 + d_5^2 - \underline{y}'^2 = 0, \tag{28}$$

$$\tilde{g}_{\overline{y}'}(d_4,d_5) = (d_4 - e\overline{y}')^2 + d_5^2 - \overline{y}'^2 = 0, \tag{29}$$

Eqs.28 and 29 represent two circles about the point (d_4, d_5) whose centers are $(e\underline{y}', 0)$ and $(e\overline{y}', 0)$, and whose radii are $\underline{y}'$ and $\overline{y}'$ respectively. The solutions of these two equations depend on the parameters e, $\underline{y}'$, and $\overline{y}'$. In our analyses, it is assumed that $0 < e < 1$ while $\underline{y}'$ and $\overline{y}'$ have opposite signs with the same magnitude. This assumption is reasonable since it requires having a hovering zone that is centered about $y = 0$. In this case, there will always be two solutions that are at the intersections of two circles. In the x-z plane, the equations are,

$$\tilde{g}_{\underline{x}'}(d_1,d_2,d_3) = \hat{g}_{\underline{x}} = 0, \tag{30}$$

$$\tilde{g}_{\overline{x}'}(d_1,d_2,d_3) = \hat{g}_{\overline{x}} = 0, \tag{31}$$

$$\tilde{g}_{\underline{z}'}(d_1,d_2) = d_1^2 + d_2^2 - \underline{z}'^2 = 0, \tag{32}$$

$$\tilde{g}_{\overline{z}'}(d_1,d_2) = d_1^2 + d_2^2 - \overline{z}'^2 = 0, \tag{33}$$

As for the in-plane direction, Eqs.32 and 33 can also be interpreted as the equations of two circles centered at $(0,0)$. If $\underline{z}'$ and $\overline{z}'$ have opposite signs but the same magnitude, all points on these circles satisfy these two conditions. Owing

to this assumption the z coordinate of the center of the periodic orbit will also be 0. Conversely, for the x states, the problem will become to find a point (d_1, d_2) on the circle described by Eqs. 32 (or 33) that satisfies both Eqs.30 and 31 with set $(\underline{x}', \overline{x}')$. Unfortunately, these equations can not always be satisfied for a random combination of $(\underline{x}', \overline{x}', \underline{z}', \overline{z}')$ because the in-plane coordinates are coupled as seen in Eq.8. Instead of directly solving Eqs. 30-33 for (d_1, d_2, d_3), this paper introduces an algorithm summarized in Algorithm 2 to obtain a feasible set of parameters. This procedure aims to find a periodic orbit with an x coordinate of the center that is close to a desired location while minimizing x-range excursion based on the given z boundaries.

Algorithm 2 Solve a periodic orbit with given magnitude of y and z orbit boundaries $[y', z']$ and initialized x orbit boundaries $[\underline{x}, \overline{x}]$

Input: Eccentricity of leader: e. The expected x-center of periodic orbit: x_c.
The boundary values: $[\underline{x}, \overline{x}, -y', y', -z', z']$.
Output: The vector of parameters $\boldsymbol{D}$ of solved periodic orbit.

$d_0 = 0$;
For y state: Solve equations 28 and 29 to get (d_4, d_5).
if $0 < e < 1$ **then**
    The assumption of $(-y', y')$ causes $d_4 = 0$. d_5 has two solutions with same magnitude but opposite sign;
else if $e = 0$ **then**
    The solutions of (d_4, d_5) are points on the circle of $d_4^2 + d_5^2 = y'^2$.
end if
Begin optimization problem to keep the x coordinate of the center of the target orbit close to x_c while minimizing the range $[\underline{x}, \overline{x}]$:
while the stopping criterion is not met **do**
    Select a set of parameters (d_1, d_2, d_3) with lower boundary $(-z', -z', \underline{x})$ and upper boundary $(z', z', \overline{x})$;
    Solve Eq.21 to retrieve the the maximum and minimum real roots: $[x_l, x_u] = polynomial_x(e, d_1, d_2, d_3)$;
    Compute the cost function $\|x_l - x_u\|^2 + (\zeta \|(x_l + x_u)/2 - x_c\|)^2$; ζ is a weight factor to balance the need to constrain the x-range of the orbit (first term) with the distance of its center from a desired position (second term).
    Impose equality constraints: $d_1^2 + d_2^2 = z'^2$;
    Impose inequality constraints: $\underline{x} \leq x_l \leq \overline{x}$; $\underline{x} \leq x_u \leq \overline{x}$; $\underline{x} < d_3 < \overline{x}$.
    Adapt the set of parameters (d_1, d_2, d_3) according to optimizer.
end while
$\boldsymbol{D} = [d_0, d_1, d_2, d_3, d_4, d_5]$.

The decision to minimize the amplitude of the target relative trajectory in the x variable stems from a sensitivity analysis, revealing that the hovering boundary region is consistently violated in the $\boldsymbol{i}$ direction of the LVLH frame unless y and z boundaries of the periodic orbit are sufficiently close to the boundaries of the hovering zone. Additionally, as the size of the relative orbit increases, the amplitude of the relative perturbations also grows, resulting in a faster drift. According to Eq.7 there are no theoretical limits to the minimum size of the relative periodic orbit that can be achieved. By setting all parameters $\boldsymbol{D} = 0$ apart from d_3 the relative trajectory is constrained to periodically oscillate along the $\boldsymbol{i}$ direction only. However, reducing the size of the orbit too much is not viable for the specific problem addressed in this paper. In fact, It is crucial to ensure that the follower spacecraft has a sufficient variation in viewing angle relative to the leader during inspections. Moreover, for some specific sensors used for relative navigation it is paramount to grant some out-of-plane motion in order to retain observability of relative states [31]. Therefore, setting adequate orbit

boundary values requires a balance of different task demands. In the effort to extend the drift duration, it is desirable to locate the x of the center of the relative periodic orbit as far as possible in the opposite direction of the drift caused by perturbations. Consequently, we adopt the conservative choice of setting x_c as the center of the hovering zone.

B. Selection of optimal target point

After a target periodic orbit is designed, the target point on it should also be selected to provide it to the optimal control module designed in Sec. III. Therefore, the optimal target point on the desired periodic orbit should be evaluated considering the fuel cost and the drift time. The exact drift time can be obtained by simulating the disturbed dynamics until the boundary of the hovering region is reached. However, this procedure is extremely time-consuming and, therefore, not suitable for onboard computation. As a consequence, an estimation method based on a short-term propagation of disturbed dynamics is exploited to approximately predict the drift time. The devised approach is not only fast but also reliable to estimate an optimal target point compared to the numerical simulations. This approach relies on heuristics that emerged after an extensive preliminary study of the effects of perturbations on various points of a target orbit. Results from several propagations indicated that the average drift velocity imposed by J_2 perturbation alone does not depend on time. In contrast, a short-term estimation of the average drift velocity caused by drag perturbation alone is not representative of the drift obtained after longer propagations. Indeed, the drift velocity imposed by drag seems to accumulate almost linearly over time, regardless of the initial point of the propagation on the relative orbit. An example of this behavior is illustrated in Fig. 7, where the average drift position and velocity after a simulation of varying durations are presented. Considering these results, a heuristic was devised to approximate the effect of drag on the drift. In particular, it was decided to create a linearly varying average drift velocity $v_{\text{drag}} = p_1 + p_2 t$. The coefficients (p_1, p_2) can be determined by fitting this expression with the data from several pairs of drift velocity v_m and corresponding propagation time t_m obtained for one of the target points.

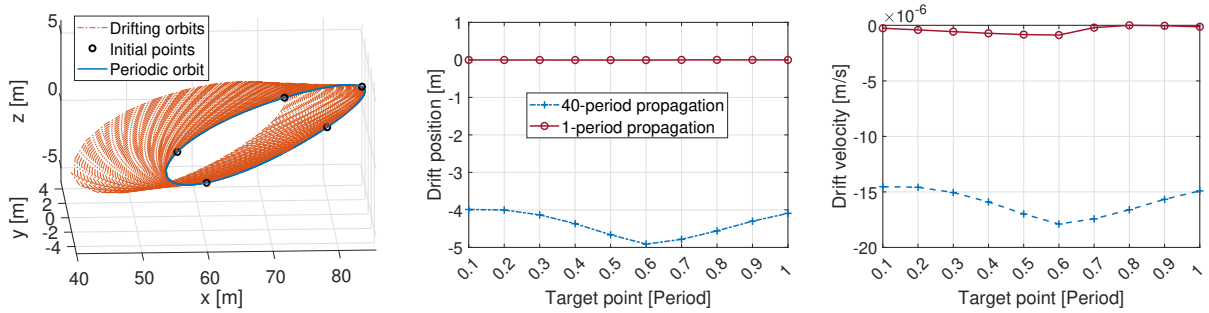

(a) Disturbed orbits from 5 different initial points (b) Drift position (c) Drift velocity

Fig. 7 Only drag perturbation.

By further assuming that the impact of perturbations could be estimated as their linear superposition (i.e., J_2 and drag separately) it was possible to devise a fast method of approximation of the total drift rate. This approach is outlined in

detail in Algorithm 3 and its comparison with the drift time obtained by the exact simulation of the perturbed dynamics for a test case is illustrated in Fig. 8. The approximated drift time shows a similar trend to the one obtained from exact simulations. Despite not predicting the correct drift time overall, this technique can be leveraged to compare target points among them and select the one that approximately provides the largest drift time while undergoing perturbed motion.

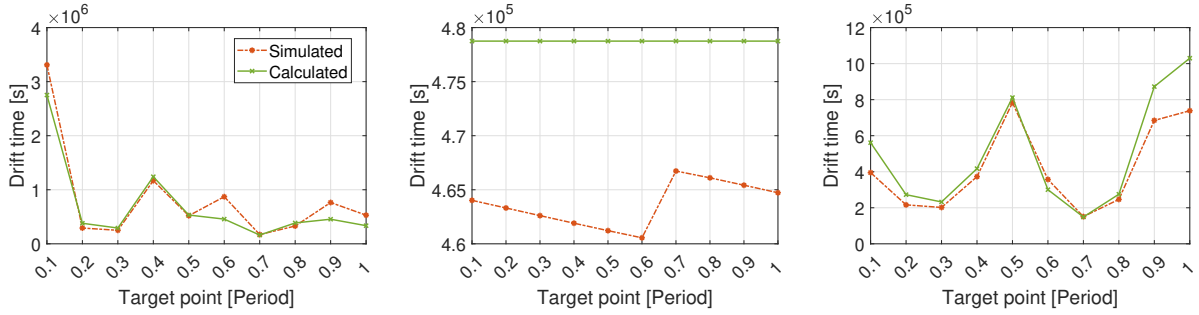

(a) Only J_2 (b) Only drag (c) J_2 and drag

Fig. 8 Comparison of simulated and calculated drift time.

The analyses conducted in this section are based on simulations where the perturbed motion starts exactly from the points on a target periodic orbit. However, as it was shown in Sec. III, for both energy-optimal and fuel-optimal control problems the target relative state cannot be reached exactly. Consequently, the periodic orbit that follows after the control phase will be different from the target one. Nonetheless, it was observed that the drift time obtained by the designed estimation method was not impacted by this error. That is an expected behavior since the drift in the $\boldsymbol{i}$ direction is the main one and the x-z orbit boundary is decoupled from the y orbit boundary. Therefore, the estimated results from the exact case, which are immediate to retrieve, can be directly applied to the tangential case for the selection of the optimal target point. To further mitigate this issue in the fuel-optimal scenario, Eqs.6 is used to convert the final relative states into the parameters $\boldsymbol{D}$, and Eqs.22, 23, 26, and 27 are included as inequality constraints of final relative states in the NLP used to solve the fuel-optimal control problem. Fig. 9 shows the effect of the application of these additional constraints to the same test case presented in Sec. III.C.

The optimal target point is not selected solely based on the maximum estimated drift time. An additional analysis for estimating the fuel cost for varying control time durations was also conducted. In Fig. 10(a), it can be observed that the cost of the transfer to different target points converges around a minimum value after a control time of nearly one period. Moreover, this trend remains consistent regardless of the shape of the leader's orbit. Therefore, there is no additional benefit in extending the control time beyond this threshold. This conclusion is further supported by examining the convergence of the NLP used for the fuel-optimal control problem. As depicted in Fig. 10(b), the algorithm struggles to converge for control durations that deviate too much from multiple integers of the orbital period of the leader. In

Algorithm 3 Approximated method to obtain the optimal target point.

Input: x boundary values of the hovering zone and the computed target periodic orbit (TPO).
Output: Estimated optimal target point.

Calculate the distance between the x boundary of the hovering zone and the TPO: d_{lower}, d_{upper}.
Choose a certain number of target points on the TPO;
For each target point, the drift velocity v_{J_2} can be computed in the same way:
Starting from chosen target points, the motion perturbed by J_2 is propagated for 1 period and its drift is averaged to obtain v_{J_2};
For each target point, the drift velocity v_{drag} is assumed to be the same:
Starting from one target point, the drag-perturbed motion is propagated to get: (v_m, t_m), $m = 1, 2, 3, \ldots$;
The average drift velocity $v_{\text{drag}} = p_1 + p_2 t$ is obtained by fitting (p_1, p_2) to the data (v_m, t_m).
for All chosen target points **do**
  if the drift direction imposed by the drag is negative **then**
    if $\left(v_{J_2} + p_1\right) \cdot t + p_2 \cdot t^2 = d_{\text{upper}}$ has a positive root **then**
      The disturbed motion arrives at the upper boundary of the hovering zone and the drift time is the positive root of this equation;
    else
      The disturbed motion arrives at the lower boundary of the hovering zone and the drift time is calculated by $\left(v_{J_2} + p_1\right) \cdot t + p_2 \cdot t^2 = d_{\text{lower}}$.
    end if
  else if the drift direction imposed by the drag is positive **then**
    if $\left(v_{J_2} + p_1\right) \cdot t + p_2 \cdot t^2 = d_{\text{lower}}$ has a positive root **then**
      The disturbed motion arrives at the lower boundary of the hovering zone and the drift time is the positive root of this equation;
    else
      The disturbed motion arrives at the upper boundary of the hovering zone and the drift time is calculated by $\left(v_{J_2} + p_1\right) \cdot t + p_2 \cdot t^2 = d_{\text{upper}}$.
    end if
  end if
end for
select the target point with longest drift time.

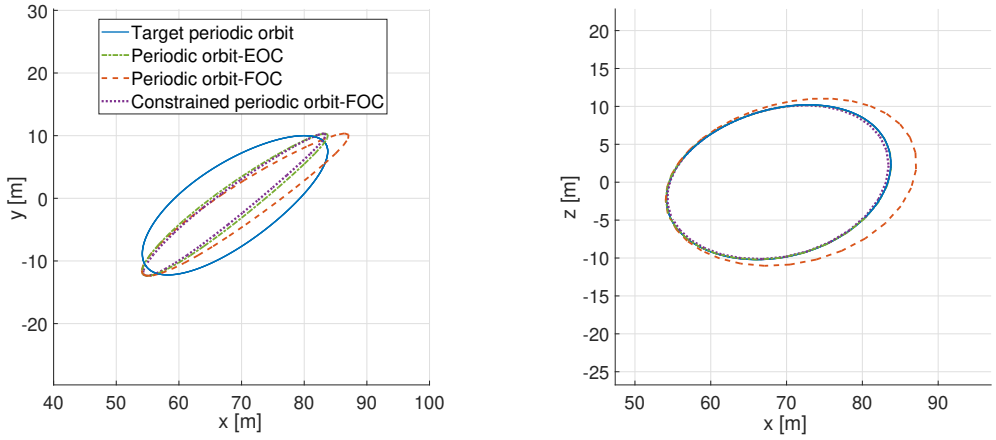

(a) x-y plane (b) x-z plane

Fig. 9 Comparison of periodic orbits for different control strategies : energy-optimal (EOC), fuel-optimal(FOC), and fuel-optimal with additional constraints.

conclusion, using longer propagation times results in larger final state errors after control. This trend is attributed to the fact that perturbations were not considered during control design, yet their presence still affects the trajectory when control is applied. This additional limitation led to the final decision to select only optimal target points that can be reached with a control duration of around one period of the leader's orbit.

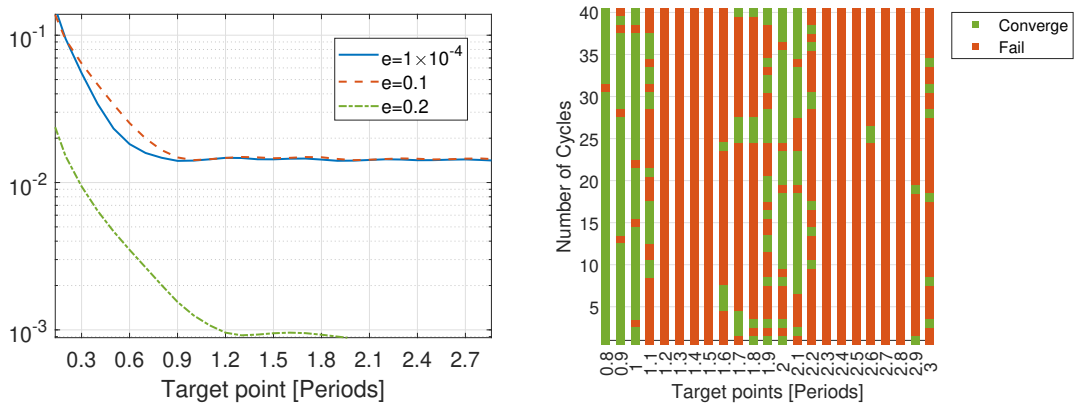

(a) Analysis of fuel cost with different orbital eccentricities. (b) Algorithm's effectiveness for different target points of 40 cycles.

Fig. 10 Motivation for the selection of 1 period control duration.

C. Numerical simulations of multiple cycles

In this section, the long-term hovering procedure is simulated in MATLAB and Simulink, with an i7-10700 2.90GHz CPU. The planning hovering horizon consists of 40 cycles within a general range of orbit eccentricity of the leader to verify the algorithm's effectiveness. Since the analyses conducted in the previous section show that the solution of the fuel-optimal control problem may not always converge, in such cases, the control obtained at the final iteration of the optimization is adopted. To understand the impact of failures in the convergence of the optimal control problem two strategies were preliminary tested. The first strategy implemented the initial guess of the optimal control problem in case of solver failures. When analyzing this approach, large final state errors appeared in relation to the desired target point of the control. These errors resulted in relative orbits that were not quasi-periodic at the end of the control phase, and hence shortened the free drift time of the follower substantially. As a consequence, it was observed that the cumulative drift time flattened with the number of hovering cycles. Moreover, the accumulated state errors caused an increase in the control effort necessary to compensate for the drift, which in turn was reflected in a sharp increase of the cumulative Δv. To sum up, an increase in cost and the constant need for replanning represent the biggest concerns for the proposed long-term hovering strategy. Conversely, the second approach adopted the control history provided by the final iteration of the nonlinear programming solver regardless of its convergence. This strategy is the one adopted to generate the results reported in this paper as it provided satisfactory performances which will be illustrated in the following.

First, the orbit eccentricity e of the leader is set at four values, 1×10^{-4}, 0.05, 0.1, and 0.2. In these cases, the maximum acceleration $a_{\max}$ is varied as $5 \times 10^{-6}\text{m/s}^2$, $1 \times 10^{-5}\text{m/s}^2$, and $1.5 \times 10^{-5}\text{m/s}^2$. The parameters for Algorithm 2 are $y' = z' = 5$ m, $x_c = 70$ m, and $\zeta = 20$. The remaining parameters are reported in Table 1. The number of cycles for which the fuel-optimal problem reaches convergence is recorded in Table 2, where it is shown that convergence can be achieved in more than 90% of the cases. The cumulative fuel cost and the cumulative drift time of these analyses are plotted in Fig 11. In these cases, it is possible to observe that the trend is approximately linear with the number of cycles. This result shows that despite the 10% of cases where the solver failed to converge, it was still possible to avoid the constant need for replanning and the associated increase in cumulative cost. Indeed, these were the two main issues that the proposed algorithm could encounter, as identified by preliminary analyses.

Table 2 Fraction of converged cycles for fuel-optimal control problem.

Maximum acceleration	Eccentricity e			
$a_{\max}(\text{m/s}^2)$	0.0001	0.05	0.1	0.2
5×10^{-6}	0.950	1	1	1
1×10^{-5}	0.925	1	1	0.950
1.5×10^{-5}	0.850	0.950	0.975	0.975

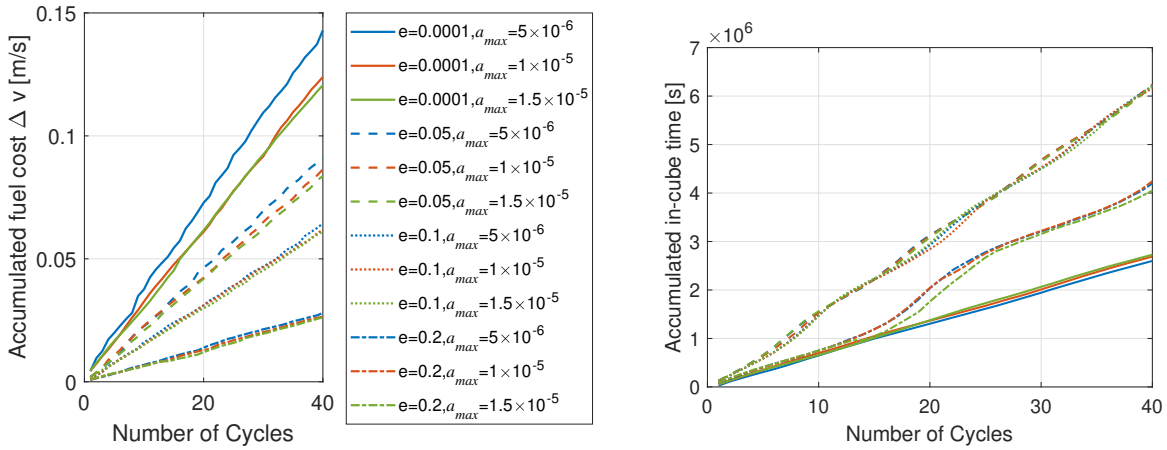

(a) Cumulative Δv (b) Cumulative drift time.

Fig. 11 The simulation results of various combinations of eccentricity and maximum acceleration.

Fig. 11(a) shows that for orbits with smaller eccentricity, the cumulative cost decreases with increasing $a_{\max}$. Moreover, the larger the eccentricity the smaller the total required cost. Conversely, the cumulative drift time reported in Fig. 11(b) does not show such trends. The cumulative drift time useful for inspection and other monitoring activities ranges from $\approx$ 70 days for orbits with very small eccentricity to $\approx$ 130 days for orbits with intermediate values of eccentricity. Overall, the average cost for a day of mission is always $\approx 10^{-3}$ (m/s)/day and it ranges from 3×10^{-4} (m/s)/day (for orbits with larger eccentricity) to $\approx 2 \times 10^{-3}$ (m/s)/day (for almost circular orbits).

During this analysis, the computational cost of the control design was also considered. Table 3 reports the average time needed for control design for the different combinations of maximum acceleration and eccentricity. Additionally, Fig. 12(a) shows the time breakdown for one of these cases: $a_{\max} = 1 \times 10^{-5}\text{m/s}^2$ and $e = 0.1$. Each bar in this figure represents the total time cost for the design of a control cycle.

Table 3 Average computational time used to design the controls of the long-term hovering strategy (40 cycles).

Maximum acceleration	Eccentricity e			
$a_{\max}(\text{m/s}^2)$	0.0001	0.05	0.1	0.2
5×10^{-6}	0.691 [s]	0.498 [s]	0.653 [s]	0.613 [s]
1×10^{-5}	0.432 [s]	0.649 [s]	0.501 [s]	0.660 [s]
1.5×10^{-5}	0.376 [s]	0.465 [s]	0.544 [s]	0.506 [s]

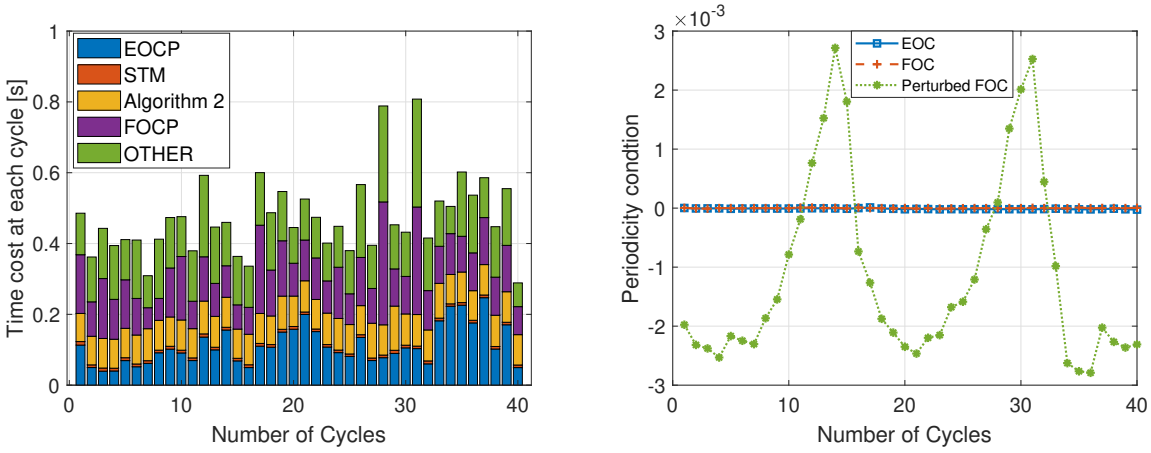

(a) Total computational time of control design at each cycle

(b) Periodicity Condition

Fig. 12 Simulation results of the case with $e = 0.1$ and $a_{\max} = 1 \times 10^{-5}\text{m/s}^2$.

It is important to notice that a big portion of the computational time is employed for interface operations ("OTHER" in Fig. 12(a)). These operations include all those complementary steps that are necessary to retrieve the final control (e.g., state conversions, mapping from time to true anomaly, etc.) but are not part of the optimization. Conversely, the time needed for the solution of the energy-optimal and of the fuel-optimal control problems (i.e., EOCP and FOCP respectively in Fig.12(a)) is limited, showing the benefit of adopting semi-analytical methods.

Moreover, Fig. 12(b) shows the final periodicity condition error obtained from the different steps of the control design. Both fuel-optimal and energy-optimal controls (i.e., FOC and EOC respectively in Fig.12(b)) are designed with unperturbed dynamics, therefore they can satisfy the final periodicity condition. However, the designed control is applied in a simulator including perturbations, which causes a final state error. Despite the presence of perturbations that are not accounted for during control design, the final periodicity condition error is still deemed acceptable (i.e., in the order of 10^{-3}). In the course of many analyses conducted during the development of this work it was observed that

small violations of the periodicity condition (i.e., in the order of 10^{-6}) produced drift times of ≈ 30 periods or more (on average). With an error of 10^{-3}, the average drift time dropped to ≈ 20 periods, as illustrated in this paper. Finally, for final errors in the periodicity condition of 10^{-2} or more, the drift time fell below 5 periods on average. This outcome constitutes a significant result of the trade-off analysis between the need to reduce control time to avoid accumulation of perturbations while also having enough flexibility to reduce the maneuver cost and increase the drift time.

V. Conclusion

This paper addresses the challenging problem of devising a long-term control strategy for hovering in proximity to a target spacecraft. To achieve this feat, the paper presents a solution through several building blocks. Initially, two semi-analytic control strategies are derived, considering thrust constrained along the tangential direction. These strategies offer a control law suitable for satellites with limited actuation capacity.

Although the control design phase neglects the effects of perturbations, the results demonstrate that for short propagation times, perturbations have a negligible impact on relative trajectories. However, tangential control does not bound the out-of-plane motion of the follower, potentially leading to violations of the hovering region in this direction during extremely long hovering missions, which are not addressed in this work.

Subsequently, the paper introduces a strategy for selecting a bounded periodic orbit that maximizes residence time within the predefined hovering region, enabling longer operations. This involves determining relative orbital parameters that constrain the orbit within the hovering zone through spatial constraints defined by polynomial inequalities. Additionally, a fast approach for evaluating the optimal target point on a periodic orbit is provided. The analyses suggest that a control duration of one period offers a promising candidate for fuel-optimal control, reaching a lower bound for fuel cost with minimal errors in the controlled final states due to orbital perturbations.

All these steps are integrated into a cyclic procedure for a long-term hovering strategy, incorporating insights from previous tests. The focus on obtaining semi-analytic procedures for optimal control solutions produced a reduction of the computational effort, making the proposed strategy a promising preliminary approach for onboard application in underactuated satellites. Finally, several simulations showcase the effectiveness of the proposed methods for different magnitudes of maximum acceleration and various shapes of the leader's orbit.

References

[1] Sanchez, J. C., "Model Predictive Control Applications to Spacecraft Rendezvous and Small Bodies Exploration," Ph.D. thesis, Universidad de Sevilla, Sevilla, Spain, Sep. 2021. URL `https://hdl.handle.net/11441/130652`.

[2] Jewison, C., and Miller, D. W., "Probabilistic Trajectory Optimization Under Uncertain Path Constraints for Close Proximity Operations," *Journal of Guidance, Control, and Dynamics*, Vol. 41, No. 9, 2018, pp. 1843–1858. https://doi.org/10.2514/1.G003152.

[3] Faraco, N., Maestrini, M., and Di Lizia, P., "Instance Segmentation for Feature Recognition on Noncooperative Resident Space Objects," *Journal of Spacecraft and Rockets*, Vol. 59, No. 6, 2022, pp. 2160–2174. https://doi.org/10.2514/1.A35260.

[4] Broschart, S. B., and Scheeres, D. J., "Control of Hovering Spacecraft Near Small Bodies: Application to Asteroid 25143 Itokawa," *Journal of Guidance, Control, and Dynamics*, Vol. 28, No. 2, 2005, pp. 343–354. https://doi.org/10.2514/1.3890.

[5] Zeng, X., Gong, S., Li, J., and Alfriend, K. T., "Solar Sail Body-Fixed Hovering over Elongated Asteroids," *Journal of Guidance, Control, and Dynamics*, Vol. 39, No. 6, 2016, pp. 1223–1231. https://doi.org/10.2514/1.G001061.

[6] Jia-Richards, O., and Lozano, P. C., "Analytical Maneuver Library for Remote Inspection with an Underactuated Spacecraft," *Journal of Guidance, Control, and Dynamics*, Vol. 45, No. 4, 2022, pp. 611–622. https://doi.org/10.2514/1.G005766.

[7] Maestrini, M., and Di Lizia, P., "Guidance Strategy for Autonomous Inspection of Unknown Non-Cooperative Resident Space Objects," *Journal of Guidance, Control, and Dynamics*, Vol. 45, No. 6, 2022, pp. 1126–1136. https://doi.org/10.2514/1.G006126.

[8] Maestrini, M., De Luca, M. A., and Di Lizia, P., "Relative Navigation Strategy About Unknown and Uncooperative Targets," *Journal of Guidance, Control, and Dynamics*, Vol. 46, No. 9, 2023, pp. 1708–1725. https://doi.org/10.2514/1.G007337.

[9] Dang, Z., Wang, Z., and Zhang, Y., "Modeling and Analysis of Relative Hovering Control for Spacecraft," *Journal of Guidance, Control, and Dynamics*, Vol. 37, No. 11, 2014, pp. 1091–1102. https://doi.org/10.2514/1.G000004.

[10] Xu, H., Ye, Y., and Yang, Z., "Nonlinear Control of Underactuated Spacecraft Hovering," *Journal of Guidance, Control, and Dynamics*, Vol. 39, No. 3, 2016, pp. 685–694. https://doi.org/10.2514/1.G001306.

[11] Irvin, D. J., Cobb, R. G., and Lovell, T. A., "Fuel-Optimal Maneuvers for Constrained Relative Satellite Orbits," *Journal of Guidance, Control,and Dynamics*, Vol. 32, No. 3, 2009, pp. 960–973. https://doi.org/10.2514/1.36618.

[12] Deaconu, G., Louembet, C., and Theron, A., "Constrained Periodic Spacecraft Relative Motion Using Non-Negative Polynomials," *Proceedings of the American Control Conference*, IEEE, New York, 2012, pp. 6715–6720. https://doi.org/10.1109/ACC.2012.6314659.

[13] Deaconu, G., Louembet, C., and Théron, A., "Designing Continuously Constrained Spacecraft Relative Trajectories for Proximity Operations," *Journal of Guidance, Control,and Dynamics*, Vol. 38, No. 7, 2015, pp. 1208–1217. https://doi.org/10.2514/1.G000283.

[14] Deaconu, G., "On the trajectory design, guidance and control for spacecraft rendezvous and proximity operations," Ph.D. thesis, Université Paul Sabatier-Toulouse III, Toulouse, France, Oct. 2013. URL https://hal.laas.fr/tel-00919883v1.

[15] Arantes Gilz, P. R., Joldes, M., Louembet, C., and Camps, F., "Model Predictive Control for Rendezvous Hovering Phases Based on a Novel Description of Constrained Trajectories," *IFAC-PapersOnLine*, Vol. 50, July 2017, pp. 7229–7234. https://doi.org/10.1016/j.ifacol.2017.08.1367.

[16] Arantes Gilz, P. R., Joldes, M., Louembet, C., and Camps, F., "Stable Model Predictive Strategy for Rendezvous Hovering Phases Allowing for Control Saturation," *Journal of Guidance, Control,and Dynamics*, Vol. 42, No. 8, 2019, pp. 1658–1675. https://doi.org/10.2514/1.G003558.

[17] Sanchez, J. C., Louembet, C., Gavilan, F., and Vazquez, R., "Event-Based Impulsive Control for Spacecraft Rendezvous Hovering Phases," *Journal of Guidance, Control, and Dynamics*, Vol. 44, No. 10, 2021, pp. 1794–1810. https://doi.org/10.2514/1.G005507.

[18] Roscoe, C., Westphal, J., and Mosleh, E., "Overview and GNC design of the CubeSat Proximity Operations Demonstration (CPOD) mission," *Acta Astronautica*, Vol. 153, 2018, pp. 410–421. https://doi.org/10.1016/2018.03.033.

[19] Gurfil, P., "Spacecraft Rendezvous Using Constant-Magnitude Low Thrust," *Journal of Guidance, Control, and Dynamics*, Vol. 46, No. 11, 2023, pp. 2183–2191. https://doi.org/10.2514/1.G007472.

[20] Maestrini, M., Di Lizia, P., and Topputo, F., "Analytical Impulsive-to-Continuous Thrust Conversion in Linearized Relative Dynamics," *Journal of Guidance, Control, and Dynamics*, Vol. 44, No. 4, 2021, pp. 862–871. https://doi.org/10.2514/1.G005520.

[21] Soderlund, A. A., and Phillips, S., "Autonomous Rendezvous and Proximity Operations of an Underactuated Spacecraft via Switching Controls," *AIAA SCITECH 2022 Forum*, 2022. https://doi.org/10.2514/6.2022-0956.

[22] De Vittori, A., Palermo, M. F., Di Lizia, P., and Armellin, R., "Low-Thrust Collision Avoidance Maneuver Optimization," *Journal of Guidance, Control, and Dynamics*, Vol. 45, No. 10, 2022, pp. 1–15. https://doi.org/10.2514/1.G006630.

[23] Arantes Gilz, P. R., "Embedded and validated control algorithms for the spacecraft rendezvous," Ph.D. thesis, Université Paul Sabatier-Toulouse III, Toulouse, France, Oct. 2018. URL https://hal.laas.fr/tel-01922288.

[24] Arantes Gilz, P. R., "A Matlab®/Simulink® Non-Linear Simulator for Orbital Spacecraft Rendezvous Applications," , Dec. 2016. URL https://hal.archives-ouvertes.fr/hal-01413328.

[25] Tschauner, J., "Elliptic Orbit Rendezvous," *AIAA Journal*, Vol. 5, No. 6, 1967, pp. 1110–1113. https://doi.org/10.2514/3.4145.

[26] Yamanaka, K., and Ankersen, F., "New State Transition Matrix for Relative Motion on an Arbitrary Elliptical Orbit," *Journal of Guidance, Control, and Dynamics*, Vol. 25, No. 1, 2002, pp. 60–66. https://doi.org/10.2514/2.4875.

[27] Bombardelli, C., Ba'u, G., and Pel´aez, J., "Asymptotic solution for the two-body problem with constant tangential thrust acceleration," *Celestial Mechanics and Dynamical Astronomy*, Vol. 110, No. 3, 2011, pp. 239–256. https://doi.org/10.1007/s10569-011-9353-3.

[28] De Vittori, A., Omodei, M., Di Lizia, P., Armellin, R., Gago, P., Torras Ribell, M., Antón, J., and Antón, D., "Numerical efficient low-thrust fuel-optimal collision avoidance maneuvers with tangential firing," *2023 AAS/AIAA Astrodynamics Specialist Conference*, 2023.

[29] Bryson, A., *Applied Optimal Control: Optimization, Estimation and Control*, CRC Press, 1975, Chap. 2, pp. 65–69. URL https://books.google.it/books?id=P4TKxn7qW5kC.

[30] Omodei, M., "Numerically efficient methods for collision avoidance maneuver design with bang-bang control," Master's thesis, Department of aerospace science and technology, Politecnico di Milano, Milan, Italy, Oct. 2022. URL https://www.politesi.polimi.it/handle/10589/195348.

[31] Woffinden, D. C., and Geller, D. K., "Relative Angles-Only Navigation and Pose Estimation For Autonomous Orbital Rendezvous," *Journal of Guidance, Control, and Dynamics*, Vol. 30, No. 5, 2007, pp. 1455–1469. https://doi.org/10.2514/1.28216.